Preparation of lanthana-doped titania nanoparticles with anatase mesoporous walls and high photocatalytic activity

Tianyou Peng [a,*], De Zhao [a], Haibo Song [a], Chunhua Yan [b]

[a] Department of Chemistry, Centre of Nanoscience and Nanotechnology Research, Wuhan University, Wuhan 430072, China
[b] State Key Laboratory of Rare Earth Materials Chemistry and Applications, Peking University, Beijing 100871, China

Abstract

Lanthana-doped mesoporous TiO_2 nanoparticles with high specific surface area and thermal stable anatase wall was synthesized via hydrothermal process by using cetyltrimethylammonium bromide (CTAB) as surfactant-directing agent and pore-forming agent. The resulting materials were characterized by XRD, FESEM, TEM, FT-IR spectroscopy, and nitrogen adsorption. The as-synthesized mesoporous doped TiO_2 nanoparticles have mean diameter of 20 nm with mean pore size of 2.2 nm. The specific surface area of the as-synthesized mesoporous nanosized doped TiO_2 exceeded $460 \, m^2/g$, and that of the samples after calcination at 500 °C still have $243 \, m^2/g$. Compared with undoped sample and P25, the lanthana-doped mesoporous TiO_2 nanoparticles show better activities on the oxidation of rhodamine B (RB). The large surface area and more active sites for combining with RB due to the present of lanthanum ion can explain the high photocatalytic activity of lanthana-doped mesoporous TiO_2 nanoparticles.
© 2005 Elsevier B.V. All rights reserved.

Keywords: Lanthana doped; Mesoporous materials; Titania; Nanoparticles; Anatase

1. Introduction

Mesoporous and nanosized TiO_2 has been a long sought after materials because of its applications in the areas of photocatalysis, solar energy conversion, and battery applications [1–5]. Among three crystalline phases of TiO_2, nanosized anatase TiO_2 is believed to possess enhanced photocatalytic activity and photoelectrical chemical conversion activity [1,2]. Therefore, there are numerous investigation focused on the synthesis of anatase nanoparticles with various shapes for the photocatalysis and photoelectrode materials [3,4]. Among those reports, the sol–gel technique is the most frequent applied. Generally, the precipitates derived from sol–gel processes are amorphous in nature [5], the photocatalytic and photoelectrical chemical conversion efficiencies of those obtained TiO_2 nanoparticles are not high enough for industrial purposes [6]. Hence, there are two

main methods developed to improve this situation, such as increasing the surface area, modification of the TiO_2 doped with metal or other semiconductors.

For the high surface area, mesoporous TiO_2 has attracted much attention due to its high surface-to-volume ratio and offers more active sites, which are of great importance in photocatalysis and solar energy conversion [7–12]. Therefore, surfactants [7,8], triblock copolymer [9], and many non-surfactant organic compounds [10] had been used as directing agent and pore-forming agent to prepare mesoporous TiO_2. In those investigation, several different approaches have been applied to control the high reactivity of Ti(IV) precursors such as non-hydrolytic routes [9], ligand-assisted templating [12], the addition of chelating agents [13], and high acidity [7,12–15]. Whereas, uncontrolled hydrolysis and condensation lead to the formation of a dense, poorly structured inorganic network. For example, Blanchard et al. have used protons in acid media to retard the rapid condensation and generate titanium mesostructured oxosulfates in a $TiOSO_4$/CTAB composite system, in which

* Corresponding author. Tel.: +86 2787218474; fax: +86 2768754067.
E-mail address: typeng@whu.edu.cn (T. Peng).

cetyltrimethylammonium bromide (CTAB) was used as surfactant-directing agent and pore-forming agent of mesoporous TiO$_2$ (but not nanoparticles) [14,15]. However, the obtained semicrystalline embedded in the amorphous mesoporous TiO$_2$ have insignificant photocatalytic activity [16]. Calcination at high temperature may not be beneficial for improving the photocatalytic activity as it results in the collapse of mesoporous framework and loss of surface area due to the crystallization of TiO$_2$ [17]. Therefore, it is still a challenge to synthesize mesoporous TiO$_2$ containing the highly crystallized anatase wall and large surface area [18–20]. Furthermore, there are a few reports on the synthesis of TiO$_2$ nanoparticle with stable anatase mesoporous framework [20a,c], which would have an advantage in relate to photocatalytic and photoelectrical chemical properties.

Together with the crystal structure, the crystalline sizes and the morphology of the individual particles, and integration of dopants in the structural framework play the key role for the optimization of specific photoelectrical chemical and catalytic properties. Therefore, numerous approaches have been conducted to extend the photoresponse of TiO$_2$ and to improve its photocatalytic activity by modifying its surface properties and composition, etc. [1,21–24]. Doping of the crystalline matrix with transition metal ions has been proven to be a potential route for the improvement of photocatalytic activity of TiO$_2$ [22–24]. Lanthanide ions are known for their ability to form complexes with various Lewis bases (e.g., acids, amines, aldehydes, alcohols, thiols, etc.) in the interaction of these functional groups with the f-orbitals of lanthanides [25–28]. Stucky and co-workers [28] has proved that the europium ions are located in glassy amorphous titania regions near the interface between the anatase nanocrystallites, and the well-ordered mesostructure is preserved. Therefore, it is expected that incorporation of lanthanide ions into TiO$_2$ matrix could not only provide a means to concentrate the organic pollutant at the semiconductor surface, but also stabilize the mesostructure, therefore, provide high surface area and enhanced photocatalytic activity of TiO$_2$ [19]. Furthermore, it has been reported that post-hydrothermal treatment of sol–gel derived gels can be applied to crystallize amorphous TiO$_2$ into anatase and stabilize mesoporous structure TiO$_2$ [20]. Here, we apply a hydrothermal method to synthesize lanthana-doped mesoporous anatase TiO$_2$ nanoparticles by using cetyltrimethylammonium bromide (CTAB) as a surfactant-directing agent and pore-forming agent in a facile and reproducible way, which is similar with our recent publication [20c]. Hydrothermal treatment and lanthanum doping are helpful to crystallize mesoporous wall into anatase and stabilize the mesoporous structure. The obtained lanthana-doped anatase TiO$_2$ nanoparticles with mesostructures show high photocatalytic activity on the oxidation of rhodamine B (RB) in air. The photocatalytic activity of the doped samples obtained exceeded that of unpoded samples and commercial Degussa P25.

2. Experimental section

2.1. Preparation and characterization

All chemical reagents used in the present experiments were obtained from commercial sources as guaranteed-graded reagents and used without further purification. A typical synthesis process for the preparation of mesoporous TiO$_2$ nanoparticles with anatase wall as follows: 1.1402 g Ti(SO$_4$)$_2$ was dissolved into 3.5 ml distilled water. The obtained solution was added into cetyltrimethylammonium bromide (CTAB) solution under stirring. The molar ration of Ti(SO$_4$)$_2$:La(NO$_3$)$_3$:CTAB:H$_2$O is 0.95:0.05:0.12:100, then adjusted the pH 0.6. After stirring for 30 min, the resulting mixture was aged at room temperature for 12 h, and then transferred into an autoclave at 100 °C for hydrothermal treatment. After 72 h, the resulting powders were cooled to room temperature, then recovered by centrifugation, washed with water and ethanol, and then dried at 120 °C overnight. In order to remove organic materials, ion-exchange treatment was performed by mixing the as-synthesized powders with a water and ethanol (molar ratio 1:1) solution of sodium chloride under stirring at 313 K for 5 h. The resulting solids were washed with water and ethanol then dried at 120 °C overnight. The as-prepared samples were calcined at different temperatures 2 h to improve crystallinity with a heating rate of 2 °C/min, respectively. The undoped samples were also prepared through a similar process [20c].

Field emission scanning electron microscopy images were obtained on a JSM-7400F (FESEM) electron microscope. Transmission electron microscopy images were obtained on a JEM-100X/II (TEM) and LaB6 JEM-2010(HT)-FEF (HRTEM) electron microscope with energy dispersive X-ray (EDX) measurements. X-ray diffraction (XRD) patterns were obtained on XRD-6000 diffractometer using Cu Kα as radiation. The nitrogen adsorption and desorption isotherms at 77 K were measured on a Micrometrics ASAP 2010 system after samples were degassed at 120 °C. IR spectra on pellets of the samples mixed with KBr were recorded on a FT-IR-8201 PC spectrometer.

2.2. Measurement of photocatalytic activity

The photocatalytic activity experiments on the mesoporous TiO$_2$ nanoparticles for the oxidation of RB in air were performed at ambient temperature. The UV source was a 300 W Hg lamp (100 mm long) with a maxium emission at approximately 365 nm, which was surrounded by a circulating water jacket (pyrex) to cool the lamp. Typically, the aqueous RB/TiO$_2$ suspension was prepared by addition of TiO$_2$ (50 mg) to a 50 ml aqueous solution containing RB dye ($c_0 = 1.0 \times 10^{-5}$ M, pH 6.0). All runs were conducted at ambient pressure and temperature. The distance between the Hg lamp and the reactor was 30 cm for each experiment. The suspension was magnetically stirred before and during illumination. The suspension was mixed for 15 min in the dark

(for the adsorption of dye onto the photocatalyst surface) and then the reaction mixture was exposed to the UV–vis light. After irradiation and removal of the TiO_2 particles by centrifugation, the residual RB was analyzed using a Shimadzu UV-240 spectrophotometer. For comparison, undoped samples and commercial catalyst Degussa P25 have also been conducted under identical experimental conditions.

3. Results and discussion

The low-angle XRD patterns of the obtained doped samples are shown in Fig. 1A. Except for the samples calcined at 900 °C, all patterns are similar and exhibit a single diffraction peak corresponding to *d*-spacing of 5.67, 5.59, 5.53 and 5.48 nm, respectively. This single strong diffraction peak in the low-angle region indicated the presence of mesostructure. Mesostructures with more or less regular diameter channel packed at random often display a single peak in low-angle XRD [20]. Compared to the as-synthesized sample, the considerable broadening and reduction in the intensity of pattern of the calcined samples, as well as the shifting of *d*-spacing to lower distances, can be attributed to the partial collapse of the mesostructure upon calcination. A single broad peak is observed on low-angle XRD patterns even for the sample calcined at 700 °C, suggesting the considerably high thermal stability of the mesostructure. The nanocrystalline walls in the obtained TiO_2 nanoparticles have been characterized by high angle powder X-ray diffraction (Fig. 1B). The as-synthesized TiO_2 powders show broad anatase peaks

(Fig. 1B (a)), indicating that the as-synthesized sample is anatase phase (JCPDS, No. 21-1272). After heat treatment, only peaks of anatase phase that become stronger and sharper are identified in Fig. 1B (b–d). Even calcination at 900 °C for 2 h, the XRD pattern show that the main crystal phase is still anatase, and small peaks of rutile phase appeared.

The average size of nanocrystallite calculated from the Scherrer formula are 2.3, 3.1, 4.5 and 6.9 nm for the samples as-synthesized and calcined at 300, 500 and 700 °C (Ref. Table 1), respectively. After calcination at 900 °C, the crystalline size increases to 8.6 nm. It has been proved that the SO_4^{2-} anion and the acidic reaction condition (pH $\sim$ 0.6) in the hydrothermal condition can retard the formation of rutile and the growth of crystal [29], and the retarded phase transformation and crystal growth in return are beneficial for high thermal stability of mesostructure and anatase. Zhang and Banfield had proved that though rutile is the most stable phase for bulk materials, when a large amount of surface is present (such as for nanoparticle smaller than 14 nm), anatase is stabilized, minimizing the total free energy of the system [29,30]. Moreover, Mayo and co-workers has also proved that the presence of interagglomerate pores can also prevent the anatase grain growth [31]. Therefore, the stabilization of the anatase phase and mesostructure upon calcinations probably can be ascribed to the present specific synthesis conditions, which are similar with our recent publication [20c].

Fig. 2 shows FESEM images of the samples as-prepared and calcined at 300 °C. As can be seen, the as-synthesized sample has a particle diameter in the range of 6.7–35 nm with mean particle size of 20 nm. After calcinations at 300 °C, the
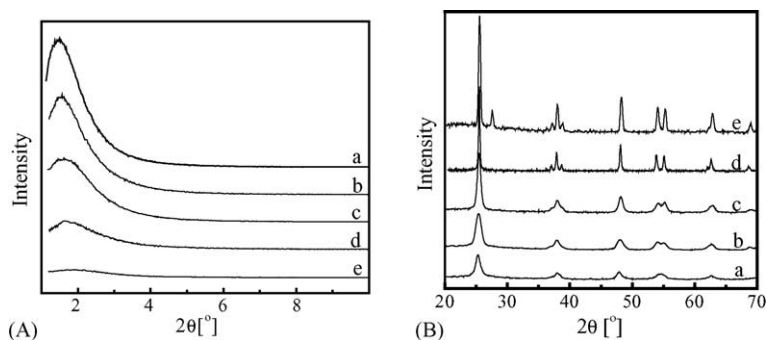

Fig. 1. Low-angle (A) and high-angle (B) X-ray diffraction (XRD) patterns of samples: (a) as-synthesized and calcined at (b) 300 °C, (c) 500 °C, (d) 700 °C, (e) 900 °C.

Table 1
Summary of the properties of mesoprous doped and unpoded TiO_2 nanosized powders[a]

Calcination temperature (°C)	Crystal size[b] (nm)	S_{BET}[c] (m²/g)	Mean pore size[d] (nm)	Total volume[e] (cm⁻³/g)
As-synthesized	2.3(2.3)	460.6(438.3)	2.2(2.1)	0.59(0.56)
300	3.1(2.9)	376.2(330.5)	2.5(2.3)	0.62(0.59)
500	4.5(4.1)	243.0(232.7)	3.0(2.5)	0.56(0.53)
700	6.9(7.3)	102.1(84.6)	–	0.39(0.32)

[a] The data in bracket is that of undoped samples.
[b] Calculated by the Scherrer equation.
[c] BET surface area calculated from the linear part of the BET plot.
[d] Estimated using the desorption branch of the isotherm.
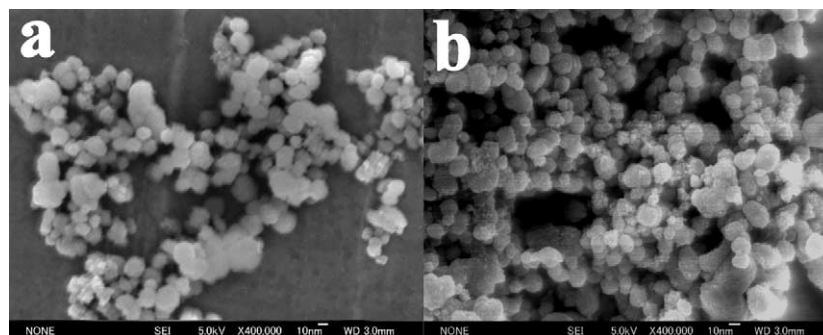[e] Single-point total pore volume of pores at $P/P_0 = 0.98$.

Fig. 2. FESEM images of the obtained samples: (a) as-synthesized and (b) calcined at 300 °C.

sample has particle size in the range of 6.5–33 nm with mean particle size of 18.5 nm. The more detailed microstructure of the nanoparticles can be seen from the TEM images (Fig. 3) of samples. The La^{3+} ion existed in the wall of the obtained samples is confirmed by energy dispersive X-ray spectroscopy (EDX) measurement (Fig. 3g). Mesoporous structure without long-range order can be clearly observed in the obtained samples, which coincides with the result of the low-angle XRD. The morphologies of pores and particles are not changed significantly upon heating up to 500 °C, indicating that reconstruction and/or collapse are not occurred drastically upon calcinations, although it can be observed that some particles have been cracked from the image of the sample calcined at 500 °C (Fig. 3e). After calcinations at 900 °C, the anatase crystallites begin to grow extensively and transform to rutile phase, and then segregate from the mesostructures. Subsequently, the whole mesostructure is completely destroyed (Fig. 3f).

From the HRTEM of the as-synthesized mesoporous sample (Fig. 3b), it is can be clearly observed that the anatase phase has already formed in the mesoporous wall. The inserted electron diffraction patterns in Fig. 3d also indicate that the crystallinity of anatase phase in the mesoporous wall is very high, which is consistent with XRD patterns of TiO_2 (Fig. 1B (b)). As can be seen from Fig. 3a–e, the pore size and the wall thickness of the as-synthesized and calcined mesoporous TiO_2 nanoparticles are estimated to be 1.6–3.9 and 2.0–5.2 nm, respectively. The estimated wall thickness excellently coincides with the anatase nanodomains (2.3–4.5 nm, estimated according to the Scherrer equation) as described above, also implying that the crystallinity of anatase in the mesostructure of the as-synthesized sample is very good (Fig. 3d). In previous work with PEO-based surfactants, Yang et al. [9] found that these crystalline domains were embedded in the mostly amorphous TiO_2 matrix. Cabrera et al. also reported 3 nm anatase in the mesoporous walls of a wormlike material [13]. In the present CTAB-templated TiO_2 system, however, the mesoporous wall basically composed of nanocrystalline with limited amount of amorphous TiO_2 matrix, implying that the hydrothermal treatment can efficiently crystallize the inorganic walls into anatase phase without destroying the mesostrucutre.

The FT-IR spectra of the obtained samples are shown in Fig. 4. It is believed that the broad peaks at 3400 and 1638 cm^{-1} correspond to the surface-adsorbed water and hydroxyl groups [7,19]. The decrease in the intensities of these peaks in the spectrum of the samples with increased calcinations temperature confirms the diminishing the surface-adsorbed water and hydroxyl groups. The peaks at 460, 620 and 910 cm^{-1} in the range of 400–1000 cm^{-1} are contribution from the anatase phase [7,19,22]. The intensities of this large band of the as-synthesized sample enhanced insignificantly upon thermal treatment, implying the anatase phase has already formed in the as-synthesized samples, which is consistent with the observation of XRD.

The N_2 adsorption–desorption isotherms and the pore size distributions of the obtained samples are shown in Fig. 5. All samples show an isotherms of type IV N_2 adsorption–desorption isotherms with hysteresis loops, clearly indicating the mesoporous nature of TiO_2, but the considerable hysteresis loop at high relative pressures confirm that the mesopores were not too regular in the obtained samples. While considering that the mesopores and nanoparticles coexist in the obtained samples, it would be reasonable to think that the hysteresis loops can be attributed to the total contribution of both intra-particle pores and inter-particle pores. The inserted pore size distribution of the as-synthesized sample determined from BJH desorption isotherm show a bimodal pore size distributions consist of smaller (1.8–5.0 nm) intra-particle pores and larger (12–52 nm) inter-particle pores. The intra-particle pore size is in range of 1.8–5.0 nm with mean pore diameter distribution at 2.2 nm, as was observed from HRTEM (Fig. 3). Moreover, the grain size becomes larger and mesopores begin to partly collapse upon calcinations, which results in the intra-particle pore size shifting to a larger mesoporous region. The sample calcined at 300 °C still maintains relatively narrow intra-particle pore size distribution. While after calcination at 500 °C, the intra-particle pore becomes weaker. It can be ascribed to the collapse of the intra-particle pores and the crystal growth. However, the pore size distribution of the inter-particle pores just changed slightly upon cacination, indicating that the inter-particles pores as well as the particle sizes changed insignificantly.
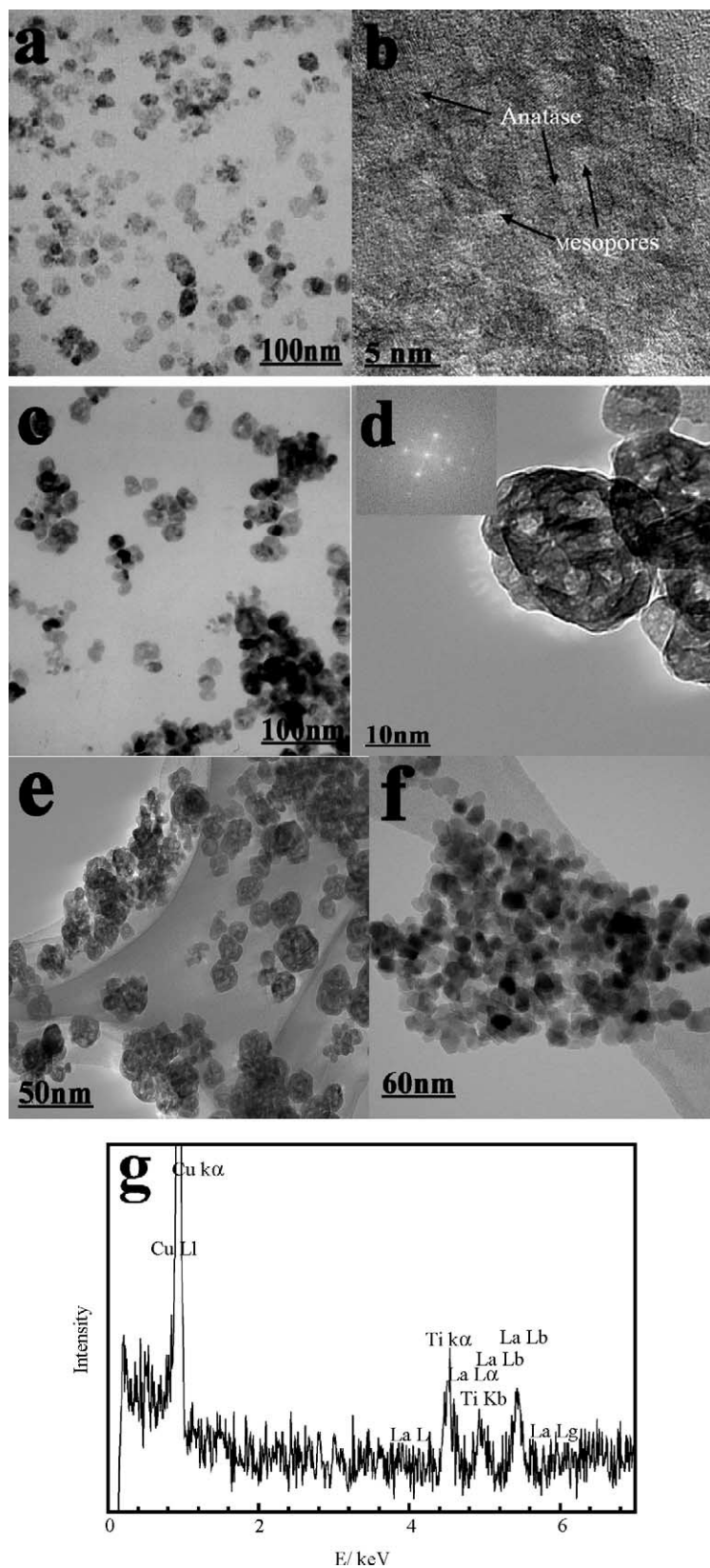
Fig. 3. TEM and HRTEM images of the mesoporous lanthana-doped TiO$_2$ nanoparticles: (a), (b) as-synthesized; (c), (d) calcined at 300 °C, (e) 500 °C, (f) 900 °C, and (g) EDX spectrum of the obtained La–TiO$_2$ samples.
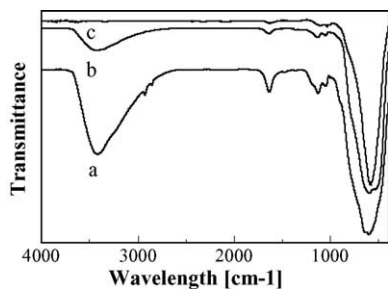
Fig. 4. FT-IR spectra of samples: (a) as-synthesized, and calcined at (b) 300 °C, and (c) 500 °C.

Fig. 6. The photocatalytic properties of doped and undoped TiO_2 samples as-prepared and calcined at different temperature as well as the P25 nanoparticles (RB, $c_0 = 1.0 \times 10^{-5}$ M, pH 6.0) after 90 min UV-light radiation.

The Brunauer–Emmett–Teller (BET) specific surface areas and pore volumes of doped and undoped samples are summarized in Table 1. Compared with the undoped samples, the relative high surface area of doped sample confirms that the frameworks of mesoporous TiO_2 have better thermal stabilities. This may be attributed to the presence of lanthanum oxide distributed on the TiO_2 matrix, which is beneficial for the effectively enhancing surface area of TiO_2 particles as reported by earlier studies [25,32,33]. The La^{3+} should mainly distribute on the surface of TiO_2 because the radius (0.1016 nm) of doped La^{3+} is larger than that of Ti^{4+} (0.068 nm). The slow rate of grain growth for doped TiO_2 may be attributed to the presence of interstitial lanthanum ions due to the La^{3+} ions inhibit grain growth by restricting direct contact of grains [32]. Gopalan and Lin [33] reported the evolution of pore structure and anatase phase stability as a result of the addition of La_2O_3. The anatase phase is stable up to 650 °C, and this is explained by possible monolayer coverage of lanthana over TiO_2. Warrier and co-workers also reported that the surface area of lanthanum doped TiO_2 nanocrystalline was increased by 25% compared to undoped one. The rutile transformation temperature increased to 850 °C in the presence of La_2O_3 from that of pure TiO_2 at 650 °C [25]. Therefore, the thermal stabilities of anatase phase and nanocrystalline sizes as well as the mesostructures of doped sample can be attributed to the lanthana doping and the existence of large amount of mesopores between the nanocrystallite wall.
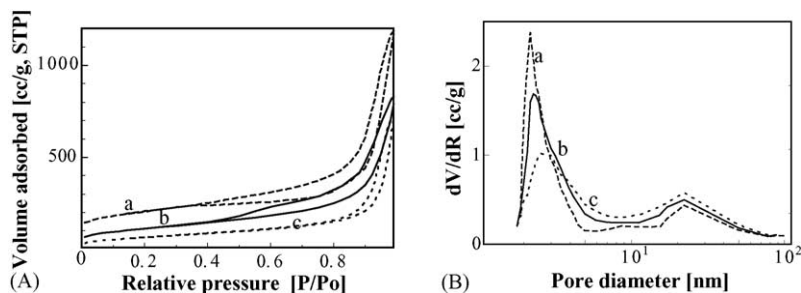
The photocatalytic activity of the obtained lanthanum doped TiO_2 nanopowders was detected by the degradation of RB aqueous solution under UV irradiation. For comparison, the photocatalytic activity of the undoped samples and commercial P25 was also measured under identical conditions. The experimental results clearly demonstrate that the degradation of RB is increased upon prolong the irradiation time. Fig. 6 shows the degradation rates of various samples after 90 min irradiation. Compared with undoped samples and P25, the optimum reactivity is observed at the doped sample calcined at 300 °C, which causes 94% RB to be degraded after 90 min irradiation. The photoactivity gradually decreased with further increases in calcinations temperature. However, all of the doped and undoped samples show better activity than Deguess P25. The improved photocatalytic activity should have some implications for the specific microstructures in the present route, which will be discussed preliminarily in the following section.

4. Discussion

There is no any ordered mesophase observed in the present system. The previous results on ordered mesophase and/or mixed mesophase, however, has been reported in many papers along with the titania/CTAB literature [7,8,14,15]. It was shown that in a $TiOSO_4$/CTAB composite mesophase, the

Fig. 5. N_2 adsorption–desorption isotherms and Barret–Joyner–Halenda (BJH) pore size distribution plots of the obtained lanthana-doped samples: (a) as-synthesized, and calcined at (b) 300 °C, (c) 500 °C.
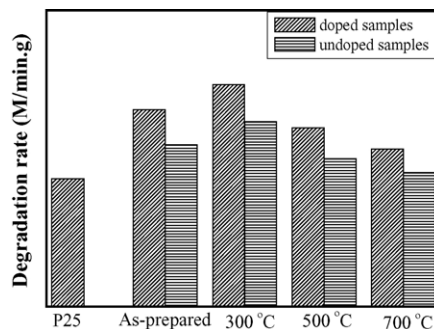
initial step is a rapid formation (<300 ms) of either a pure lamellar, hexagonal, or a mixed mesophase with a low degree of condensation, depending on the chain length of the surfactant as well as on the ionic strength of the solution [14,15]. However, due to the present closed hydrothermal experiment, in which the initial reactants and the final products was present at pH < 1, as well as the lower concentration of surfactant, we can only obtain the nanoparticles with disordered mesostructure rather than long-range ordered mesophase [20c].

The surface areas and pore sizes of the obtained samples allow for comparison with previous work: Antonelli and Ying [34] ($200 \, m^2 \, g^{-1}$, 3.2 nm, calcined at $400 \,°C$), Stone and Davis [8] ($300 \, m^2 \, g^{-1}$, 2.4 nm, calcined at $400 \,°C$), Blanchard et al. [15] ($350 \, m^2 \, g^{-1}$, 2.1 nm, calcined at $350 \,°C$). It is well known that a large amount of uncondensed Ti–OH exists on the surface of the amorphous mesoporous TiO_2. During calcination, the rapid reactions between the uncondensed Ti–OH would cause the walls of mesoporous TiO_2 to collapse. It has been reported that post-hydrothermal treatment of sol–gel derived gels can be applied to crystallize amorphous TiO_2 into anatase and stabilize mesoporous structure TiO_2 [20]. In the present work, the hydrothermal treatment is also beneficial for crystallizing porous wall into the anatase and effectively increasing its thermal stability, thus preventing the mesopores from collapse. The obtained materials present some useful characteristics for the photocatalysis, such as the large and accessible pore surfaces, small crystal size and high crystallization of anatase mesoporous wall etc. Therefore, it is worthy to further discuss the reason of the high photocatalytic activity of the obtained samples here.

The mechanism of TiO_2-photocatalyzed reactions has been the subject of extensive research [25–27,35]. It is widely recognized that the surface-adsorbed water and hydroxyl groups can act as photoexcited hole traps on the catalyst surface and produce hydroxyl radicals, which are powerful oxidants in degrading organics [21,35]. For effective degradation, the organic material should be pre-concentrated at the semiconductor surface in order to effectively trap the respective reactive radicals. Concentration of the organic compounds at the semiconductor surface has been achieved by selective doping of the semiconductor [26]. Lanthanide ions are known for their ability to form complexes with various Lewis bases in the interaction of these functional groups with the f-orbitals of the lanthanides. Warrier et al. [25] also reported that the lanthana-doped TiO_2 can provide more adsorption sites, making them more efficient catalysts. The enhanced photocatalytic activities of TiO_2 doped by rare-earth oxides such as europium, praseodymium, and ytterbium oxides were also reported [26]. Also, Lin and Yu [27] reported the effect of the addition of Y_2O_3, La_2O_3, and CeO_2 on the photocatalytic activities of TiO_2 for the oxidation of acetone. Therefore, compared with that of undoped samples and P25, the enhancement of degradation activity of doped samples are probably contributed by the larger surface areas, and the lanthanum doping in our obtained nanosized samples, which

can supply a great number of the surface states available to adsorb hydroxide and combine with RB.

By examining the photocatalytic activity changes at different temperatures, this clear enhancement of degradation rate, however, is probably not just a consequence of enrichment of RB at the surface of mesoporous nanosized TiO_2. It can be found that the photocatalytic activity increased when the calcination temperature is increased to $300 \,°C$. Compared with the as-synthesized sample, the sample calcined at $300 \,°C$ possesses reduced surface area but a more excellent crystallinity, as indicated in Fig. 1 and Table 1. Therefore, we think that the degree of crystallinity also played an important role in the photoactivity of TiO_2. Previous researchers showed that polycrystalline samples of TiO_2 have high photodegradation rates as compared with amorphous forms [36]. Ohtani et al. determined that the photocatalytic activity of TiO_2 with a constant particle size increased linearly with the fractional crystallinity of anatase [16]. Apparently, crystallinity and photoactivity are inextricably linked. While the photodegradation activity slightly reduced when the calcination temperature is increased from 300 to $500 \,°C$. This reduction of photocatalytic activity may be attributed to the extensive decreases of specific surface area, as described in Table 1. Together with the reduction of surface areas, the crystalline growth of anatase probably brings about the activity reduction of samples caicined at above $500 \,°C$. Based on above discussion, it would be reasonable to conclude that the high photocatalyitc activity of the doped mesoporous TiO_2 nanoparticles calcined at $300 \,°C$ can be attributed to larger surface area and more active sites for combining with RB due to the present of lanthanum ion in the TiO_2 mesostructure. Further studies are necessary to clarify the effects of the surface area, doping, microstructure, and crystalline composition of TiO_2 on the photocatalytic activity.

5. Conclusions

Mesoporous lanthana-doped TiO_2 nanosized powders with high surface area and stable anatase wall was prepared by using CTAB as directing-agent and pore-forming agent via a hydrothermal processes. Most organic compounds in mesoporous nanosized powders could be removed by anion-exchange process. Hydrothermal treatment crystallized powders into anatase without destroying the mesostructure and increased the surface area of the powders significantly. The obtained mesoporous doped TiO_2 nanopowders exhibits higher photocatalytic activity than the undoped sample and P25. The high photocatalytic activity of the calcined mesoporous lanthana-doped TiO_2 nanosized powders is related to its larger surface area, as well as more active sites for combining with organic compound due to the present of lanthanum ion in the high thermal stable mesostructures TiO_2. The La_2O_3 doped mesoporous materials with anatase wall presented here could have potential for use in photocatalysis, photoelectrocialchemical applications.

Acknowledgments

References

[1] M.R. Hoffmann, S.T. Martin, W. Choi, D.W. Bahnemann, Chem. Rev. 95 (1995) 69.
[2] Y.T. Kwon, K.Y. Song, W.I. Lee, G.J. Choi, Y.R. Do, J. Catal. 191 (2000) 192.
[3] P.W. Morrison, R. Ragahavan Jr., A.J. Timpone, C.P. Artelt, S.E. Pratsinis, Chem. Mater. 9 (1997) 2702.
[4] Y. Murakami, T. Matsumoto, Y. Takasu, J. Phys. Chem. B 103 (1999) 1836.
[5] C.C. Wang, J.Y. Ying, Chem. Mater. 11 (1999) 3113.
[6] C.N. Rusu, J.T. Yates, Langmuir 13 (1997) 4311.
[7] G. Soler-Illia, A. Louis, C. Sanchez, Chem. Mater. 14 (2002) 750.
[8] V.F. Stone Jr., R.J. Davis, Chem. Mater. 10 (1998) 1468.
[9] P. Yang, D. Zhao, D.I. Margolese, B.F. Chmelka, G.D. Stucky, Nature 396 (1998) 152.
[10] (a) C. Wang, Q. Li, R.D. Wang, Mater. Lett. 58 (2004) 1424;
(b) J.Y. Zheng, J.B. Pang, K.Y. Qiu, Y. Wei, J. Mater. Chem. 11 (2001) 3367.
[11] D. Khushalani, G.A. Ozin, A. Kuperman, J. Mater. Chem. 9 (1999) 1491.
[12] H.S. Yun, K. Miyazawa, H.S. Zhou, I. Honma, M. Kuwabara, Adv. Mater. 13 (2001) 1377.
[13] S. Cabrera, J. El-Haskouri, A. Beltran-Portier, D. Beltran-Portier, M.D. Marcos, P. Amoros, Solid State Sci. 2 (2002) 513.
[14] M. Linden, J. Blanchard, S. Schacht, S. Schunk, F. Schuth, Chem. Mater. 11 (1999) 3002.
[15] J. Blanchard, F. Schuth, P. Trens, M. Hudson, Microporous Mesoporous Mater. 39 (2000) 163.
[16] B. Ohtani, Y. Ogawa, S.I. Nishimoto, J. Phys. Chem. B 101 (1997) 3746.
[17] S.H. Elder, Y. Gao, X. Li, J. Liu, D.E. McCready, C.F. Windisch, Chem. Mater. 10 (1998) 3140.
[18] L.M. Huang, Q.Z. Li, Chem. Lett. 28 (1999) 829.
[19] J.C. Yu, L.Z. Zhang, Z. Zheng, J.C. Zhao, Chem. Mater. 15 (2003) 2280.
[20] (a) Y.D. Wang, C.L. Ma, X.D. Sun, H.D. Li, Mater. Lett. 54 (2002) 359;
(b) T.Y. Peng, A. Hasegawa, J.R. Qiu, K. Hirao, Chem. Mater. 15 (2003) 2011;
(c) T.Y. Peng, D. Zhao, K. Dai, W. Shi, K. Hirao, J. Phys. Chem. B 109 (2005) 4947, and the references therein.
[21] J.C. Yu, L.Z. Zhang, J.G. Yu, Chem. Mater. 14 (2002) 4647.
[22] K.E. Karakitsou, X.E. Verykios, J. Phys. Chem. 97 (1993) 1184.
[23] W. Choi, A. Termin, M.R. Hoffmann, Angew. Chem. Int. Ed. Engl. 33 (1994) 1091.
[24] T. Lopez, J. Hernandez-Ventura, R. Gomez, F. Tzompantzi, E. Sanchez, X. Bokhimi, A. Garcya, J. Mol. Catal. A: Chem. 167 (2001) 101.
[25] C.P. Sibu, S. Rajesh Kumar, P. Mukundan, K.G.K. Warrier, Chem. Mater. 14 (2002) 2876.
[26] (a) K.T. Ranjit, E. Joselevich, I. Willner, J. Photochem. Photobiol. A: Chem. 96 (1996) 185;
(b) K.T. Ranjit, H. Cohen, I. Willner, S. Bossmann, A. Braun, J. Mater. Sci. 34 (1999) 5273;
(c) K.T. Ranjit, I. Willner, S.H. Bossmann, A.M. Braun, Environ. Sci. Technol. 35 (2001) 1544.
[27] (a) J. Lin, J.C. Yu, J. Photochem. Photobiol. A: Chem. 116 (1998) 63;
(b) J. Lin, J.C. Yu, D. Lo, S.K. Lam, J. Catal. 183 (1999) 368.
[28] K.L. Frindell, M.H. Bartl, M.R. Robinson, G.C. Bazan, A. Popitsch, G.D. Stucky, J. Solid State Chem. 172 (2003) 81.
[29] H. Zhang, J.F. Banfield, J. Mater. Chem. 8 (1998) 2073.
[30] E.L. Crepaldi, G.J.de A.A. Soler-IIIia, D. Grosso, F. Cagnol, F. Ribot, J. Am. Chem. Soc. 125 (2003) 9770.
[31] S.L. Liao, K.D. Pae, W.E. Mayo, Nanostruct. Mater. 3 (1995) 319.
[32] X.Z. Ding, X.H. Liu, J. Mater. Res. 13 (1998) 2556.
[33] R. Gopalan, Y.S. Lin, Ind. Eng. Chem. Res. 34 (1995) 1189.
[34] D.M. Antonelli, Y.J. Ying, Angew. Chem. Int. Ed. Eng. 34 (1995) 2014.
[35] T. Nakahira, M. Gratzel, J. Phys. Chem. 88 (1984) 4006.
[36] R.S. Davidson, C.L. Morrison, J. Abraham, J. Photochem. 24 (1994) 27.